Journal of Physics: Condensed Matter

PAPER • **OPEN ACCESS**

Li 1*s* core exciton in LiH studied by x-ray Raman scattering spectroscopy

To cite this article: O A Paredes-Mellone *et al* 2019 *J. Phys.: Condens. Matter* **31** 055501

OPEN ACCESS
IOP Publishing
Journal of Physics: Condensed Matter
J. Phys.: Condens. Matter **31** (2019) 055501 (9pp)
https://doi.org/10.1088/1361-648X/aaf24c

Li 1s core exciton in LiH studied by x-ray Raman scattering spectroscopy

O A Paredes-Mellone[1,2], G E Stutz[1,2], S A Ceppi[1,2], P Arneodo Larochette[3], S Huotari[4] and K Gilmore[5]

[1] Facultad de Matemática, Astronomía, Física y Computación (FaMAF), Universidad Nacional de Córdoba (UNC), 5000 Córdoba, Argentina
[2] IFEG, CONICET-UNC, FaMAF, 5000 Córdoba, Argentina
[3] CONICET—Centro Atómico Bariloche (CNEA), 9500 S.C. de Bariloche, Argentina
[4] Department of Physics, PO Box 64, FI-00014 University of Helsinki, Finland
[5] ESRF—The European Synchrotron, CS 40220, 38043 Grenoble Cedex 9, France

E-mail: oparedes@famaf.unc.edu.ar and stutz@famaf.unc.edu.ar

Received 2 October 2018, revised 14 November 2018
Accepted for publication 20 November 2018
Published 19 December 2018

Abstract

The Li 1*s* core excitation spectra in LiH was studied by means of x-ray Raman scattering (XRS) spectroscopy in a wide range of momentum transfers q. The analysis of the near-edge region of the measured spectra in combination with q-dependent *ab initio* calculations of XRS spectra based on the Bethe–Salpeter equation (BSE) reveals that the prominent peak at the excitation onset arises from two main contributions, namely a pre-edge peak associated to a p-type core exciton and strong transitions to empty states near the bottom of the conduction band, which is in contrast to previous experimental studies that attributed that feature to a single excitonic peak. The p-like angular symmetry of the core exciton is supported by BSE calculations of the relative contributions to the XRS spectra from monopole and dipole transitions and by the observed decrease of its normalised intensity for increasing momentum transfers. Higher energy spectral features in the measured XRS spectra are well reproduced by BSE, as well as by real-space multiple-scattering calculations.

Keywords: x-ray Raman scattering, core-exciton, lithium hydride

(Some figures may appear in colour only in the online journal)

1. Introduction

Lithium hydride is the simplest heteronuclear compound; it crystallises in the simple rock-salt structure and in the unit cell it has only four electrons, which have *s*-like character in a picture of essentially ionic bonding between Li^+ and H^-. This simplicity has led the use of LiH as a benchmark to probe different theoretical approaches for electronic structure calculations [1]. More recently, a renewed interest in studying the electronic structure and optical properties of light metal hydrides [2, 3] has grown due to their potential application as hydrogen storage materials [4].

Lithium halides, in general, have been taken as prototype compounds to investigate excitonic states [5–7]. In particular, excitonic effects in the electron excitation spectra of LiH have been the subject of several experimental studies. Valence excitons have been observed in optical measurements [8], where the ground and the first excited state of the optical exciton could be clearly resolved in the reflection spectrum at the fundamental edge [9–11]. A first experimental sign for core-hole excitonic effects in LiH was provided by measurements of the reflectance spectrum at the Li K-absorption edge [12]. Based on similarities with the absorption spectrum of LiF, a prominent peak at the onset of the reflectance spectrum was attributed to a transition from the Li^+ 1*s* level to a $n = 1$ core-exciton state associated with the p-like conduction band. Prominent peaks observed in the photoelectron yield spectrum [13] and in the electron energy-loss spectrum (EELS) [14] at

the Li K-edge were also assigned to a core exciton, though discrepant energy positions were reported in the different works. The energies of the exciton resonances were evaluated in several studies on the electronic structure of LiH by means of different theoretical approaches. While results from Hartree–Fock (HF) calculations of energy bands are in poor agreement with experimental data, even when correlations and relaxation corrections are considered [15], quasiparticle band structure calculations including many-body effects in the Coulomb-hole-plus-screened-exchange approximation [16] predicted quantitative results in better agreement with the experiments. More recently, calculations of the Li 1s near-edge absorption spectra of lithium halides [17], including effects of electron-core hole interactions, predicted a strong excitonic peak at the onset of the spectra and succeed in reproducing nearly all spectral features. For the particular case of LiH, Shirley [17] pointed out that the core-exciton seems to be merged with the continuum portion of the spectrum. On the contrary, all the lithium halides exhibit a single prominent excitonic peak in the pre-edge region of the Li K-edge absorption spectra. This would indicate that the first peak observed in reflectance [12], photoelectron yield [13] and EELS [14] measurements at the Li K-edge might not be ascribed to a pure excitonic peak.

Core-level spectroscopic techniques offer element-specific information by directly probing atomic core-levels of a specific element present in the sample under study. In particular, inelastic x-ray scattering (IXS) by core-electron excitations, also known as x-ray Raman scattering (XRS), is a powerful tool for probing excited electronic states [18, 19]. This technique is based on measuring the energy-loss spectrum of scattered hard x-rays, while transferring momentum and energy to the scattering electron system. The advantage of this non-resonant spectroscopic technique is that the incident photon energy can be freely chosen and thus low-energy absorption edges can be investigated using hard x-rays, thus avoiding all constraints inherent to UV/soft x-ray spectroscopies. In addition, XRS provides true bulk information and makes it possible to study systems in specific sample environments. Since the momentum transfer can be freely varied, transitions other than the dipolar ones are able to be probed, which allows excited electronic states of different symmetry to be studied. XRS spectroscopy succeeded in revealing the symmetry of core excitons in lithium fluoride [20], icosahedral boron carbide [21], diamond [22] and hexagonal boron nitride [23].

It is the aim of this work to exploit the potentiality of XRS spectroscopy, concerning the q-dependence of the cross-section, along with simulations of XRS spectra by means of calculations schemes that includes electron–hole interaction effects to provide new insights into the structure of the core-electron excitation spectra and to shed light on the excitonic features in LiH.

2. Experiment

Inelastic x-ray scattering spectra by Li 1s electron excitations in LiH were measured at the XDS beamline [24] of the Brazilian Synchrotron Light Laboratory (LNLS). Radiation generated from a 4 T superconducting wiggler was collimated by a cylindrically bent mirror (Si- or Rh-coated, depending on the operation mode) and monochromated by a liquid-nitrogen-cooled Si(1 1 1) double crystal monochromator. The first crystal is planar and the second one is cylindrically bent in order to sagittally focus the monochromatic beam onto the sample position. The monochromatic beam was further focused in the vertical direction by a cylindrically bent Rh mirror. The beam size on the sample was 0.17 mm (vertical) $\times$2.2 mm (horizontal). The sample was a LiH pellet with a thickness of 8.5 mm and a diameter of 12 mm. To avoid reactions of LiH with moist air, the sample was mounted into the scattering chamber in an Ar-filled glove box and kept in the scattering chamber under a constant flux of dry nitrogen during the measurements. No degradation of the sample surface was observed after the measurements. The spectra of inelastically scattered photons were collected using a Johann type spectrometer in Rowland geometry. A spherically bent Si(1 1 0) crystal of 420 mm curvature radius was employed to analyse and to focus the scattered radiation onto an Amptek SDD detector. The analyser was operated at a Bragg angle of 88.25°. Measurements of energy-loss scans were performed in the so-called inverse geometry, i.e. by varying the incident energy while keeping fixed the analysed energy. The scattering plane was chosen to be the horizontal plane, with a vertical analysing plane, in order to diminish the geometrical effects of the sample thickness on the energy resolution. We employed two different operation modes of the beamline during the experiment in order to cover a wide range of transferred momenta. In a low-(high-)energy mode, the analyser crystal was operated at the 440(660) reflection, which corresponds to an analysed energy of 6.46 keV(9.69 keV). The total energy resolution was 1.0 eV(1.6 eV) at the low-(high-) energy mode setting. IXS spectra for momentum transfers in the range 0.24 a.u. $\leqslant q \leqslant$ 0.84 a.u. and 0.84 a.u. $\leqslant q \leqslant$ 4.9 a.u., with a momentum transfer resolution of 0.07 a.u. and 0.2 a.u., were measured in the low- and high-energy mode, respectively.

3. Theoretical background

In an inelastic x-ray scattering process a photon is scattered from an electron system; energy and momentum are transferred to the scattering electrons and the system is left in an excited state. The measured quantity is the double differential scattering cross section (DDSC), which, for incident energy values far from any electron binding energy, can be expressed in terms of the dynamic structure factor $S(\mathbf{q},\omega)$ as [19]

$$\frac{\mathrm{d}^2\sigma}{\mathrm{d}\Omega \mathrm{d}\omega} = \left(\frac{\mathrm{d}\sigma}{\mathrm{d}\Omega}\right)_{\mathrm{Th}} S(\mathbf{q},\omega) \tag{1}$$

where the coupling of the probe with the system is described by the Thomson scattering cross section $\left(\frac{\mathrm{d}\sigma}{\mathrm{d}\Omega}\right)_{\mathrm{Th}} = r_0^2(\hat{\epsilon}_1 \cdot \hat{\epsilon}_2)\frac{\omega_2}{\omega_1}$. r_0 is the classical electron radius and ω_1 (ω_2) and $\hat{\epsilon}_1$ ($\hat{\epsilon}_2$) are the incident (scattered) photon energy and the polarisation vector of the incident (scattered) photon, respectively. The system-dependent quantity $S(\mathbf{q},\omega)$, given by [19]

$$S(\mathbf{q},\omega) = \sum_F \mid \langle F| \sum_j \exp(\mathrm{i}\mathbf{q}\cdot\mathbf{r}_j)|I\rangle \mid^2 \delta(\omega + E_I - E_F), \tag{2}$$

yields specific information about the scattering electron system, where $\omega = \omega_1 - \omega_2$ and $\mathbf{q} = \mathbf{k}_1 - \mathbf{k}_2$ are the transferred energy and momentum, respectively, during the scattering process. This factor includes all possible transitions allowed by energy conservation between initial $|I\rangle$ and final $|F\rangle$ many-body states, with corresponding energies E_I and E_F, respectively. $\sum_j$ indicates a summation over the position vectors $\mathbf{r}_j$ of all the electrons in the system.

For small momentum transfers ($qa \ll 1$, a being the Li 1s orbital radius), the transition operator $\exp(\mathrm{i}\mathbf{q}\cdot\mathbf{r})$ is reduced to the dipole operator, yielding a direct correspondence between XRS and x-ray absorption spectroscopy (XAS) [19]. At non-zero q-values, non-dipolar excitation channels become available and contribute to the measured scattered intensity. This is a unique characteristic of XRS spectroscopy.

4. Computational methods

4.1. FEFF code

One of the computational treatments of x-ray Raman scattering considered in this work is based on the FEFF package [25], an *ab initio* real space multiple scattering (RSMS) code, which was expanded to compute q-dependent XRS spectra [26, 27]. In the RSMS approach, the dynamic structure factor for the case of polycrystalline materials is reduced to the calculation of atomic transition matrix elements $M_l(q,E)$ and the local angular-momentum projected density of states (l-DOS) in the presence of the core hole $\rho_l(E)$

$$S(q,\omega) = \sum_l (2l+1) \mid M_l(q,E) \mid^2 \rho_l(E), \tag{3}$$

where $E = E_K + \omega$ is the final state photoelectron energy corresponding to the initial electronic bound state with binding energy E_K [26]. Within this picture, the measured spectrum can be analysed in terms of a linear combination of transition components corresponding to excitation channels of a given angular momentum symmetry.

In our calculations, we have used the experimental lattice parameter of 4.08 Å [28] for the fcc crystal structure of LiH. Self-consistent calculations were performed using the FEFF9.7 package utilising the Hedin–Lundqvist exchange-correlation potential for a cluster radius of 7 Å. For the near-edge region, a cluster radius of 9 Å was employed for full multiple scattering convergence and up to $l = 6$ angular momentum channels for calculation of the excitation matrix elements. Directionally averaged calculations of XRS spectra were performed for different momentum transfer values within the range 0.24 a.u. $\leqslant q \leqslant$ 4.9 a.u.

4.2. OCEAN code

LiH XRS spectra were also calculated through the OCEAN code [29, 30], which provides a package to numerically solve the Bethe–Salpeter equation (BSE) for core-level excitations. This *ab initio* code takes into account explicitly the screened interaction between the core-hole and the photo-electron in a two-particle formalism. Its primary focus is on the near-edge region of the core excitation spectrum.

Orbitals from the plane-wave DFT package QUANTUM ESPRESSO [31] were used. These calculations were performed using norm-conserving pseudopotentials and therefore both an auxiliary atomic code and a pseudopotential inversion scheme are necessary for core-level spectroscopy [29]. We employed the local-density approximation to the exchange-correlation functional and used a 100 Ry energy cut-off for the plane-wave basis. For final state wave functions a $8 \times 8 \times 8$ **k**-point sampling was found to be sufficient for convergence, whereas for screening, increasing the **k**-point grid beyond $2 \times 2 \times 2$ had no discernible effects on the calculated spectra. The electronic contribution to the static dielectric constant must be supplied to compute the long-range core-hole screening within the approach implemented in OCEAN. We found that using $\epsilon = 3.52$, which is slightly smaller than the value $\epsilon = 3.61$ obtained from the index of refraction [32], a convergence of the screened core-hole interaction for a cut-off radius of 3.5 a.u. can be achieved.

5. Data analysis

Usual energy dependent corrections due to absorption of the incident beam in beam paths, windows and sample were applied. The measured intensity of each spectrum was normalised to the monitor intensity. The extraction of the XRS spectrum from the whole electron excitation spectrum needs some care because the core spectrum is usually superimposed on a background due to the valence electron contribution, which can strongly depend on the momentum transfer. An extraction algorithm for the core electron contribution in IXS experiments was proposed by Sternemann *et al* [33]. In this work, we have followed a similar procedure for low and high momentum transfers, as discussed below; whereas for medium q-values, some modifications to that algorithm were needed in order to obtain a satisfactory extraction.

For high momentum transfers ($q \geqslant 2.6$ a.u.), the measured spectra were transformed into Compton profiles (CP) using the relativistic formulation of Ribberfors [34] within the impulse approximation. The valence electron contribution was described by an experimental CP, which was extracted from the fully corrected, spherically averaged LiH CP measured in [35]. The core-electron CP was approximated by an HF atomic CP [36]. Deviations from the impulse approximation lead generally to asymmetric Compton profiles [37]. The valence CP was corrected for asymmetry effects by means of the phenomenological function [33]

$$A(p_z) = \alpha_1 \tanh(p_z/\alpha_2) \exp[-(p_z/\alpha_3)^4] \tag{4}$$

where $\alpha_i (i = 1, 2, 3)$ are fitting parameters and p_z is the projection of the electron momentum along the direction of the momentum transfer vector. At the highest momentum transfer, deviations from the impulse approximation in the core-electron part of the spectrum cannot be properly taken into

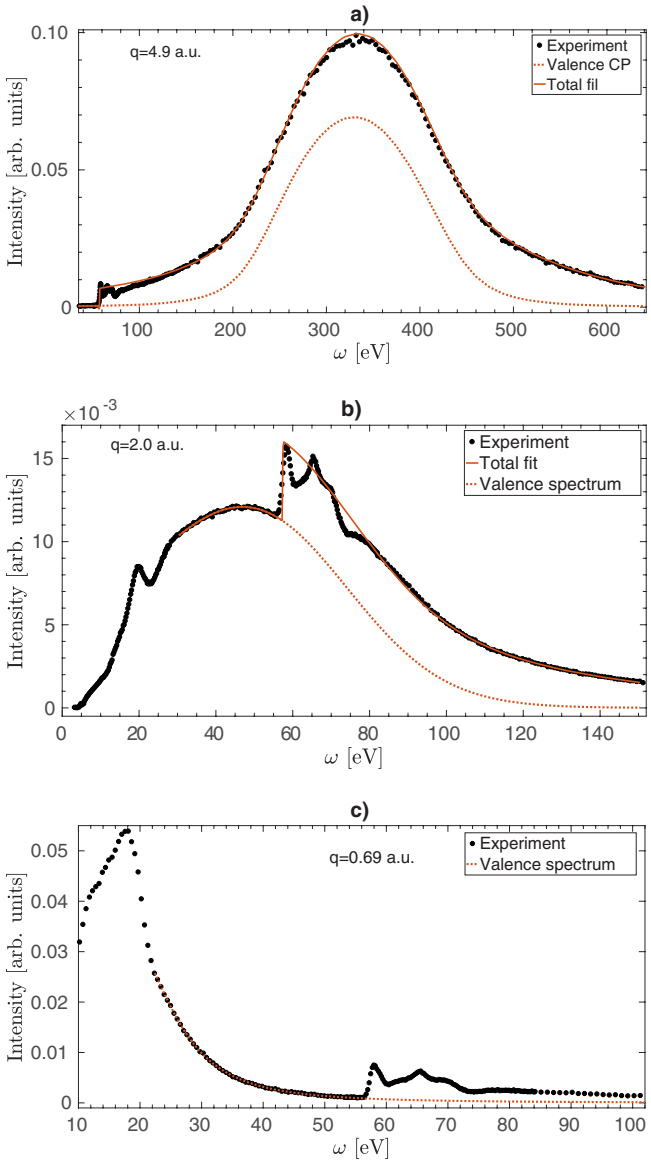

Figure 1. Measured IXS spectrum (symbols) as a function of the transferred energy for $q = 4.9$ a.u. (a), $q = 2.0$ a.u. (b) and $q = 0.69$ a.u. (c). The valence-electron contribution (dash-dotted line) and the total fit (solid line) are also shown. For the models used to describe the core and valence part of the spectrum for the different momentum transfers, see text.

account by equation (4). An explicit asymmetry-correction to the atomic HF CP was necessary in order to describe correctly the complete excitation spectrum over the whole energy range. Holm and Ribberfors [38] evaluated the first correction to the non-relativistic Compton cross section in the impulse approximation. We have applied this correction to the core CP, where the weight factor of the correction was used as a fitting parameter. The fitting procedure to extract the core-electron contribution was performed by normalising the measured spectrum to the area of the asymmetry-corrected total CP over the range -2 a.u. $< p_z < 2$ a.u. In figure 1(a) the measured and the fitted spectrum for $q = 4.9$ a.u. are shown, along with the corresponding valence component. For the other spectra within the high-q range, a similar procedure was applied, though no explicit core asymmetry correction was needed.

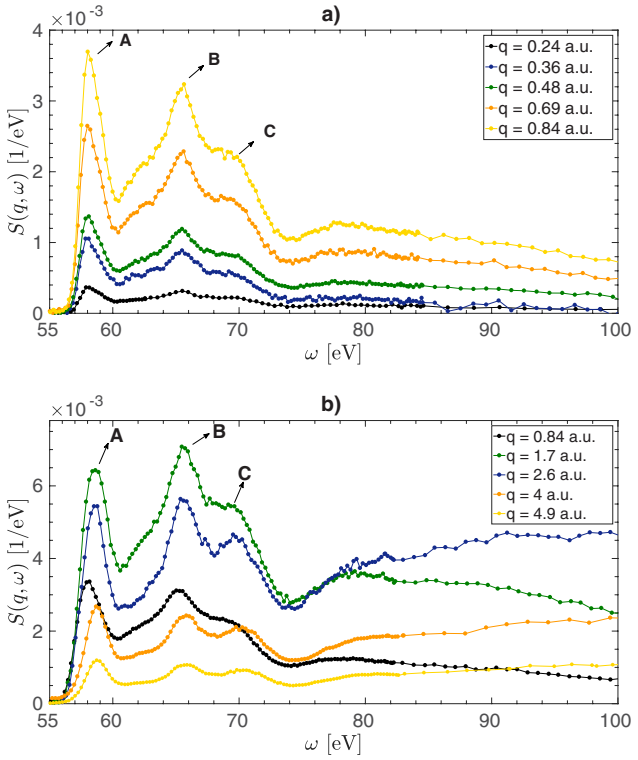

Figure 2. Extracted Li 1*s* XRS spectra of LiH for 0.24 a.u. $\leqslant q \leqslant$ 0.84 a.u., measured in the low-energy mode (a) and for 0.84 a.u. $\leqslant q \leqslant$ 4.9 a.u., measured in the high-energy mode (b). The relative experimental uncertainties, as determined from the counting statistic, at the first maximum of the XRS spectra are between 0.4 % and 1.7%.

In the region of intermediate momentum transfers (1.7 a.u. $\leqslant q \leqslant$ 2.0 a.u.), deviations from the impulse approximation are so strong that the procedure described above cannot properly account for the valence contribution to the IXS spectra. In this q-range, a phenomenological Pearson IV function

$$P_{\mathrm{IV}}(\omega) = \alpha_1 \left[1 + \left(\frac{\omega - \alpha_2}{\alpha_3}\right)^2\right]^{-\alpha_4} \exp\left[-\alpha_5 \tan^{-1}\left(\frac{\omega - \alpha_2}{\alpha_3}\right)\right], \tag{5}$$

where $\alpha_i (i = 1, \ldots, 5)$ are fitting parameters, was used to model the valence contribution, while the core electron contribution was described by an atomic CP from [36]. We found that this model allows for a very good description of the excitation spectrum within a 25 eV wide region below the Li K edge and also on the high energy tail of the spectra (see figure 1(b)).

For the lowest momentum transfers (0.24 a.u. $\leqslant q \leqslant$ 1.3 a.u.), as proposed in [33], we fit the Pearson VII function

$$P_{\mathrm{VII}}(\omega) = \alpha_1 [\alpha_2^2 (\omega - \alpha_3)^2 + 1]^{-\alpha_4}, \tag{6}$$

with $\alpha_i (i = 1, \ldots, 4)$ fitting parameters, to the measured spectra in an interval of about 30 eV at energies lower than the core excitation onset and then extrapolated the fitted function to higher energy transfers. The resulting XRS spectra (see figure 2) were obtained by subtracting the corresponding valence part from the whole energy loss spectra.

6. Results and discussion

Figure 2 shows the extracted Li 1*s* XRS spectra following the procedure presented in the previous section. The experimental XRS spectra were not measured in a sufficiently wide energy range in order to apply the sum rule to normalise them [19], in particular at the largest momentum transfers. Instead, as discussed in [22], the measured XRS spectra were brought to absolute units by normalising them to the same area of theoretical spectra in a finite energy window. In this work, the XRS spectra simulated with the FEFF code, which provides spectra in absolute units, were used to normalise the measured spectra in the energy range 55 eV $< \omega <$ 90 eV. Since the FEFF spectra satisfy the sum rule, the measured spectra become normalised according to the sum rule.

At small values of momentum transfer (figure 2(a)), several features are displayed by the experimental core excitation spectra. A prominent sharp peak (A) at ∼58 eV, a structured broader peak (B) at ∼65.4 eV, with a weak shoulder at ∼62.4 eV and a marked shoulder on its high energy side (C), at ∼69 eV, can be observed. At higher energies, a broad peak spreads over the energy region from about 75 eV–80 eV. In addition to these fine structures, a chemical shift at the Li *K* edge of about 2 eV to higher energies in relation to metallic lithium is exhibited by the measured LiH XRS spectra, which is caused by the ionic character of LiH. The observed spectral features can be identified with the main features in the reflectance spectrum at the Li *K*-edge from [12], located at 57.8 eV, 61.8 eV, 66 eV and 70.7 eV. In addition, the overall spectral shape of present XRS spectra for low momentum transfers is very similar to the imaginary part of the dielectric function determined from the reflectance spectrum. The more prominent structures (peaks A and B) were also observed in the Li *K* photoelectric yield spectrum [13] and in the electron energy-loss function [14] of LiH, but with a somewhat poorer correspondence as to their location on the energy scale. Within the range of 0.24 a.u. $< q <$ 0.84 a.u., besides the increase in spectral weight, which is determined by the normalisation assumed, no appreciable changes in the XRS spectra were observed. This suggests that for these momentum transfers the XRS spectra are dominated by contributions from dipolar excitation channels, as expected since $0.08 < qa < 0.29$ in that q-range. As the magnitude of the momentum transfer is increased beyond 0.84 a.u. (figure 2(b)), the high energy shoulder of peak B evolves into a marked peak at ∼70 eV. The position of peak A shifts towards higher energy transfers for increasing q, with a total shift of ∼0.8 eV in the measured q-range. A similar behaviour is observed for the peak B with a total shift of about ∼0.6 eV.

In figure 3 we show experimental and calculated XRS spectra for some selected q values. Instrumental broadening effects were taken into account in the calculated spectra by convolving them with a gaussian response function with a full-width at half-maximum given by the experimental energy resolution. OCEAN spectra were normalised as the experimental ones. While FEFF provides XRS spectra calculated on an absolute energy scale, OCEAN results need to be

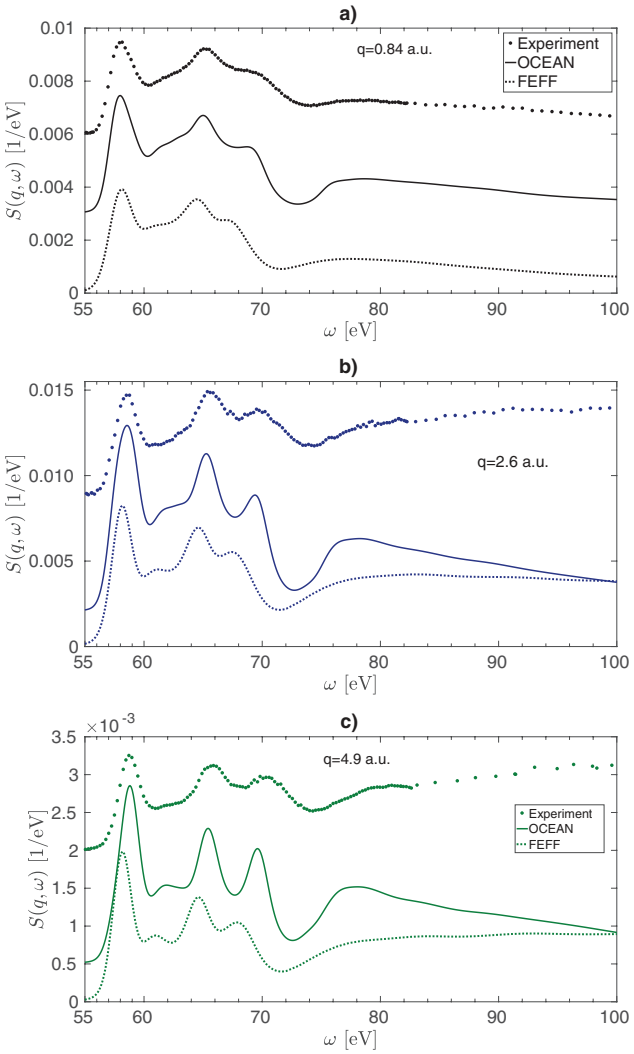

Figure 3. Experimental (symbols) and FEFF (solid line) and OCEAN (dashed line) calculated core-electron $S(q,\omega)$ for $q = 0.84$ a.u. (a), $q = 2.6$ a.u. (b) and $q = 4.9$ a.u. (c). Spectra were vertically shifted for clarity. The energy scale of the OCEAN spectra was set as discussed in the text.

shifted to allow a direct comparison with experimental data. For this purpose, a relative shift of the OCEAN spectra was introduced by aligning the first excitation peak in the calculated spectrum with the experimental peak A for the lowest q-value. The calculated spectra show overall good agreement with the experimental results and all the structures in the near-edge region are well reproduced by the results of both codes. FEFF and measured spectra are in good agreement in relation to the absolute energy position of the spectral features. The observed increase of spectral weight of the shoulder C with q is also predicted by both codes. Nevertheless, concerning the energy shift of the main features with the momentum transfer, whereas OCEAN results predict also a positive dispersion, no noticeable shift of the position of peaks A and B is predicted by FEFF. At high momentum transfers, the experimental XRS spectra show a slow intensity rise in the high-energy tail, which is qualitatively well reproduced by FEFF results. This demonstrates the robustness of the extraction algorithm across the whole investigated energy range.

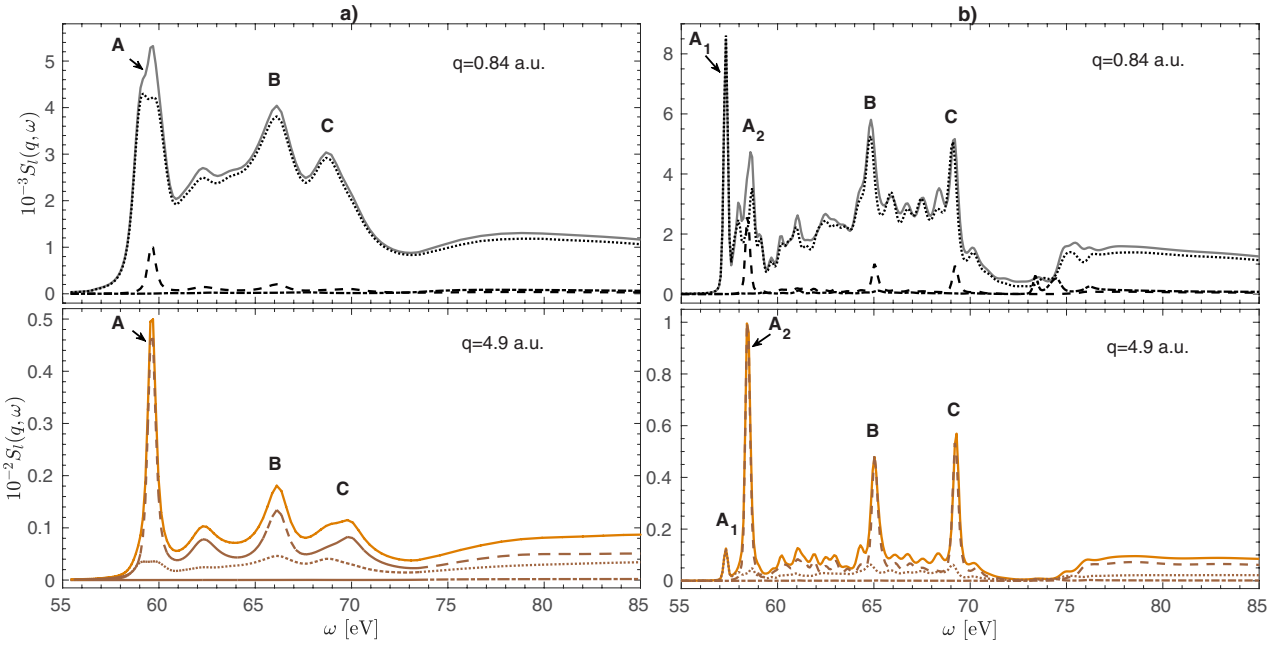

Figure 4. Li 1*s* $S_l(q,\omega)$ for monopolar (dashed line), dipolar (dotted line) and quadrupolar (dash-dotted line) excitation channels, along with the total $S(q,\omega)$ (solid line) simulated with FEFF (a) and OCEAN (b) for $q = 0.84$ a.u. and $q = 4.9$ a.u. The calculated spectra were broadened with 0.1 eV.

In order to analyse the observed spectral features in further detail, the partial contributions from the different excitation channels according to the angular symmetry of the final electronic state are shown in figure 4. In the energy region around the structure A, FEFF calculations (figure 4(a)) predict monopolar and dipolar contributions to the XRS spectra, which peak at almost the same energy. Consequently, a single non-dispersing structure of mixed *s*- and *p*-symmetry is originated. In the OCEAN spectra, besides that structure (labeled as A_2 in figure 4(b)), an additional peak (A_1) about 1 eV to lower energies is predicted. The peak A_1 is originated by transitions to final states of pure *p*-symmetry. Due to the finite instrumental resolution, the predicted double-peak structure A_1–A_2 is not resolved in the experimental spectra. At low *q*-values, the peak A_1 is more prominent than the A_2 one and the position of the experimental peak A is dominated by the former. An opposite behavior is observed for high momentum transfers. As a result, the center of gravity of the complex structure A in the experimental and in the convolved OCEAN spectra shifts slowly towards higher energies as *q* increases. This indicates that the first prominent structure in the experimental core spectra is consistent with an underlying double-peak structure, as predicted by the BSE formalism as implemented in the OCEAN code. The sharp lower-energy peak A_1 is attributed to transitions to a core exciton state of *p*-like symmetry, whereas the second peak A_2 arises from transitions from the core level to states of high density of states (DOS) in the lowest conduction bands. In the FEFF code, the core-hole interaction is treated within the final-state-rule approximation, where the quasi-particle final states are eigenstates of a Hamiltonian in the presence of a self-consistently screened core-hole muffin-tin potential. The BSE formalism considers the core-hole interaction explicitly by calculating the screened direct interaction in the static approximation [30]. Present results show that the latter treatment leads to a more complete description of the excitonic effects in LiH.

FEFF and OCEAN calculations show that structure B is also composed of excitations from core states to *s*- and *p*-like final states, but with contribution of monopolar transitions which are weaker than those for the peak A_2. A detailed inspection shows that OCEAN results predict a monopolar transition energy slightly higher than the dipolar one. As a result, peak B shifts slightly towards higher energies for increasing momentum transfers, in agreement with the experiment, while the peak B predicted by FEFF remains static. The differences between FEFF and OCEAN results can be attributed to the levels of approximation of the underlying electronic structure.

Results from both codes indicate that structure C is originated mainly by dipole-like transitions at low momentum transfers. A strong contribution from monopolar transitions rises at the same energy as *q* is increased, which is more noticeable in the OCEAN results. This explains the observed evolution of the structure C in the experimental spectra from a shoulder to a marked peak when going from low to high momentum transfers. In relation to the spectral features appearing at higher energies, the broad structure located at 75–80 eV can be assigned to transitions to states of marked *p*-character. For $q > 2.6$ a.u., monopolar transitions channels start to contribute in a wide range at higher energies, as predicted more markedly by the FEFF results, which should be responsible for the rise in spectral weight observed at the high energy tail of the XRS spectra.

In order to extract the pre-edge peak A_1 from the first structure observed in the measured XRS spectra, a fitting procedure, based on a relatively simple model, is proposed. As suggested by the OCEAN calculations of the angular-momentum

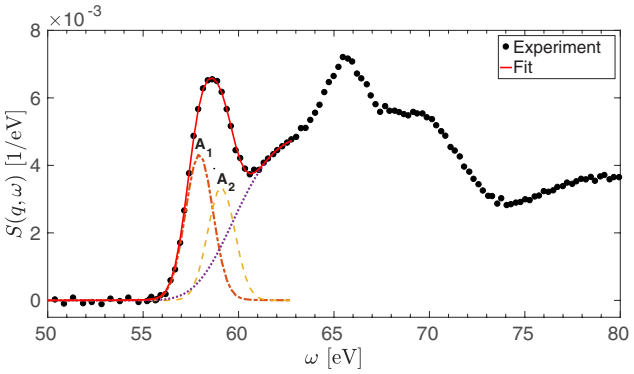

Figure 5. Fit of the near-edge structure A in the experimental XRS spectra measured at $q = 1.7$ a.u. Total and partial components of the fitting model (see text) are shown.

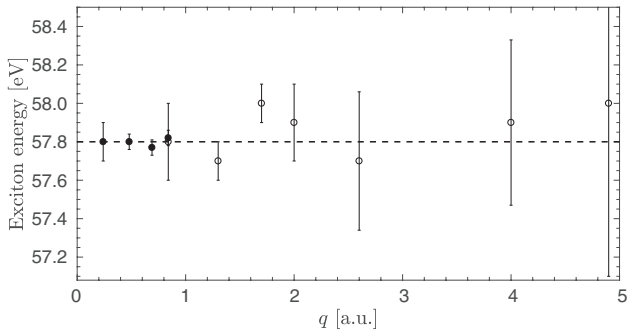

Figure 6. Energy position of the excitonic peak in the XRS spectra measured in the low-energy mode (filled circles) and high-energy mode (open circles). The dashed line shows a mean value from a weighted fit to the experimental data.

projected $S(q,\omega)$ (see figure 4), we propose a fitting model based on a two-peak structure to describe peaks A_1 and A_2, along with a tail towards lower energies to account for the continuum portion of the spectrum that is merged with the former peaks. The best fit was achieved by using a Voigt profile to describe peak A_1, where the width of the Gaussian component was set to the instrumental energy resolution, and a Gaussian function for peak A_2. The continuum part of the spectra was modeled by the low energy tail of the modified Gaussian profile

$$G_{\mathrm{mod}}(\omega) = \frac{\alpha_1}{\alpha_2\sqrt{2\pi}} \exp[-(\omega-\alpha_3)^4/(2\alpha_2^2)], \qquad (7)$$

$\alpha_i (i = 1,\ldots,3)$ being the fitting parameters. To perform the fit, we assumed that in the regions 55 eV $\lesssim \omega \lesssim$ 57 eV and 61 eV $\lesssim \omega \lesssim$ 63 eV only peak A_1 or the decaying tail of the continuum spectrum contributes, respectively. In the remaining part of the fitting interval all the three fitting functions were considered. The fitting result for the spectrum measured at $q = 1.7$ a.u. is shown in figure 5. The proposed fitting model was able to resolve a two-peak structure in the low-energy structure A of all the measured XRS spectra. Peak A_1 is associated with the Li 1*s* core exciton, whereas peak A_2 is originated by transitions from the core level to states near the bottom of the conduction band. Band structure calculations indicated that the lowest conduction band in LiH has *p* symmetry [1], however OCEAN and FEFF calculations show that some contribution from transitions to *s*-like final states exists at energies close to the core-conduction threshold (see figure 4). This contribution increases appreciably at higher momentum transfers.

The fitted position of peak A_1 is shown in figure 6 for all measured XRS spectra. The peak position shows no dispersion within experimental errors, with a mean value of (57.80 ± 0.02) eV. On the basis of HF calculations of energy bands including correlation and relaxation effects, Kunz and Mickish [15] computed the energy of the fundamental core exciton line to be 61.70 eV, which is significantly higher than the present experimental value. This discrepancy can be traced back to electronic polarisation effects that are not completely accounted for by the electronic polaron model used to include correlation effects in the calculations of [15].

A precise value for the exciton binding energy, i.e. the exciton energy relative to the bottom of the conduction band, is not possible to be determined from the experimental XRS spectra because the onset of transitions to *p*-like empty states is not distinctly resolved due to the strong superposition of A_1 and A_2 peaks. Notwithstanding, upper bounds for this energy can be estimated to 1.0 eV from the energy difference between peaks A_1 and A_2 (58.8 eV). HF-calculations from [15] predicted for LiH a Li *K*-shell band gap of 66.87 eV, from which a binding energy for the core exciton of 5.17 eV can be evaluated, in worse agrement with the experiment. Baroni *et al* [16] computed quasiparticle (QP) energy bands of LiH within the Coulomb-hole-plus-screened-exchange (COHSEX) formalism. Using the reduced mass at the point X_2 of the Brillouin zone, where the conduction band minimum occurs, and a dielectric constant of 3.61, the exciton binding energy was evaluated to be 0.70 eV [16], in close agreement with the present experimental estimate. The tendency of the HF formalism to overestimate predicted values in comparison to the experimental ones was also observed in the energy gap and the valence bandwidth of lithium hydride [16]. QP band structure calculations predict a nonrigid downward shift of conduction bands that leads to a theoretical energy threshold for core-conduction transitions of 58.82 eV [16], which is in good accordance with present experimental findings. The inclusion of many-body effects through the COHSEX approximation in the calculations by Baroni *et al* [16] was decisive in order to improve the quantitative agreement with experimental results.

In a photoelectric yield study [13], structure A was associated to a pure excitonic peak and the bottom of the conduction band was proposed to be located in the dip between peaks A and B. Under these assumptions, the first strong transition from the core-level to conduction states was associated with peak B [13, 16]. The results from the present fitting procedure, along with the OCEAN calculations, show that the higher energy peak A_2 of the structure A, instead of peak B, must be related to the first strong core-conduction transitions.

Concerning the other spectral features in the XRS spectra, according to the QP band structure calculated by Baroni *et al* [16], peaks B and C can be identified with dipole-allowed transitions to states around point X_5 (67.16 eV) and to the higher energy state L_1 (70.87 eV), respectively. The onset of

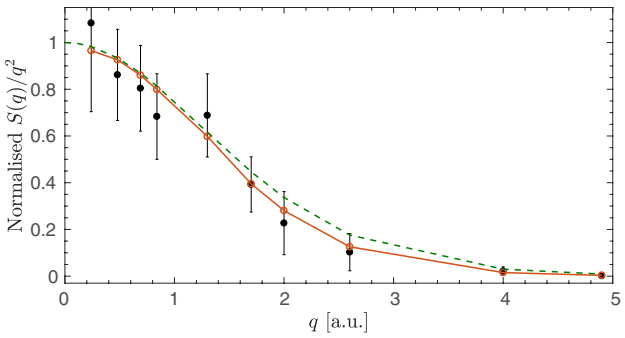

Figure 7. Normalised core exciton intensity $S(q)/q^2$ at different momentum transfers: experiment (solid circles), OCEAN calculations (open circles) and hydrogen-like model [21] (dashed line). All curves are normalised to unity at $q = 0$. Solid line is a guide to the eye.

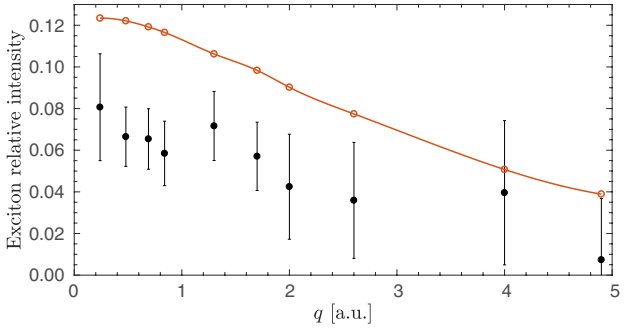

Figure 8. Core exciton relative integrated intensity at different momentum transfers: experiment (solid circles), OCEAN calculations (open circles). Solid line is a guide to the eye.

the broad structure at 75–80 eV in the XRS spectra can be related to transitions to p-like states of the conduction band at L_3 (73.11 eV) and Γ_4 (74.73 eV) points. Despite providing an accurate band gap, calculations of excited state properties within the framework of the GW-LDA and GW-GGA approximations [39] predicted underestimated electronic transition energies as compared to present experimental results. In [39] transition energies also in the COHSEX approximation were evaluated, but the predicted values are about 5 eV lower than previous COHSEX calculations by Baroni *et al* [16]. The discrepancies could be traced back to the approximations assumed in the different theoretical studies.

In relation to calculations of electronic density-of-states, the structures observed in the measured XRS spectra can be well related to states of high DOS in the conduction band of LiH, according to DOS's computed in the DFT framework using the GGA [40], EVGGA [3] and GW [41] approximations. However, some discrepancies exist in the relative position of the structures of the DOS between the different theoretical approaches.

As previously demonstrated by q-dependent XRS measurements [20–23], the q-dependence of the excitonic structure is a strong indication of the exciton symmetry. The normalised exciton intensity $S(q)/q^2$, evaluated as proposed by Feng *et al* [23], is shown in figure 7. For the sake of comparison, in addition to OCEAN results we also compute the normalised $S(q)/q^2$ as given by a simple atomic model that assumes transitions between hydrogen-like $1s$ and $2p$ states, as proposed in [21]. In order to enable a comparison between the experimental results and those obtained by the theoretical models, the value of $S(q)/q^2$ extrapolated at zero momentum transfer was set to the unity. In spite of the relatively large experimental uncertainties, originated by the strong overlap between peaks A_1 and A_2 in the measured spectra, a clear monotonic decrease in the integrated area can be observed. This decrease is a characteristic of p-type excitons, also observed in hexagonal boron nitride [23] and in icosahedral boron carbide [21]. The overall q-dependence of the experimental normalised $S(q)/q^2$ is in very good correspondence with both theoretical models, which constitutes further evidence for an exciton of p-like symmetry.

Although the curves shown in figure 7 display the overall q-dependence, the spectral weight of the excitonic structure is not reflected by the normalised $S(q)/q^2$. The intensity of the excitonic peak, relative to the integrated area of the XRS spectrum over the energy range from 55 to 90 eV, is shown in figure 8. It should be noted that the relative exciton intensity computed this way is independent of the theoretical normalisation used in this work and, particularly, of the q^2-dependence introduced by the sum rule into the first momentum of the spectra. Despite differences in the absolute values, OCEAN and experimental results show consistency in predicting a decreasing exciton spectral weight as the momentum transfer increases. OCEAN results are in average a factor two higher than the measured relative intensities. Strong overestimation of the exciton spectral weight calculated by means of the BSE formalism was also observed in different lithium halides when compared to measured absorption spectra [42].

7. Conclusions

We reported an experimental and theoretical study of the Li $1s$ core excitation spectra in LiH using XRS spectroscopy and calculations based on the RSMS and BSE methods, as implemented in the FEFF and OCEAN codes, respectively. By introducing some modifications to a previously reported data processing algorithm, originally applied to the regime of low and high momentum transfer, we were able to successfully extend its application to the intermediate q range. An analysis based on a fitting model, supported by BSE calculations, indicates that the lowest energy structure observed in the measured core excitation spectra is not a pure excitonic feature, as proposed by previous spectroscopic studies. This feature is consistent with a double-peak structure, with a peak associated with transitions from the core level to the lowest states of the conduction band and a pre-edge peak of p-type excitonic character. The upper limit for the exciton binding energy and the core-conduction excitation threshold, derived from the measured XRS spectra, are in close agreement with quasi-particle band structure calculations [16]. The overall dependence of the normalised intensity of the exciton peak on the magnitude of the momentum transfer is in good agreement with the BSE calculations, which provides conclusive evidence for the p-symmetry of the exciton. Present results

allowed to unambiguously resolve the underlying structure of the first excitation feature and the symmetry of the core exciton. Most of the observed changes in the measured XRS spectra with increasing q can be mainly attributed to a steady growing contribution of monopolar excitation channels, which dominate over the dipole-like ones at high momentum transfers. The BSE formalism implemented in the OCEAN code proved to be a fundamental theoretical tool to interpret excitonic features in the near-edge region of XRS spectra.

Acknowledgments

Research was supported by SeCyT-UNC (Universidad Nacional de Córdoba, Argentina), LNLS (Brazilian Synchrotron Light Laboratory), CNPEM/MCTI and the Academy of Finland (grant No. 1295696). Computing time at the Finnish Grid and Cloud Infrastructure (persistent identifier urn:nbn:fi:research-infras-2016072533) is gratefully acknowledged. O A P M acknowledges CONICET for a graduate fellowship and the Finnish National Agency for Education for a CIMO fellowship. Assistance from F Gennari is gratefully acknowledged.

ORCID iDs

OAParedes-Mellone https://orcid.org/0000-0002-8711-3985
S A Ceppi https://orcid.org/0000-0003-3122-0121

References

[1] Islam A K M A 1993 *Phys. Status Solidi* **180** 9
[2] van Setten M J, Popa V A, de Wijs G A and Brocks G 2007 *Phys. Rev.* **75** 035204
[3] Reshak A 2013 *Int. J. Hydrog. Energy* **38** 11946
[4] Schüth F, Bogdanović B and Felderhoff M 2004 *Chem. Commun.* **20** 2249
[5] Haensel R, Kunz C and Sonntag B 1968 *Phys. Rev. Lett.* **20** 262
[6] Pantelides S T and Brown F C 1974 *Phys. Rev. Lett.* **33** 298
[7] Tsuji J, Kojima K, Nakamatsu H, Mukoyama T and Taniguchi K 2001 *J. Synchrotron Rad.* **8** 554
[8] Plekhanov V G 1998 *Rep. Prog. Phys.* **61** 1045
[9] Plekhanov V G, Pustovarov V A, O'Connell-Bronin A A, Betenekova T A and Cholakh S O 1976 *Sov. Phys. Solid State* **18** 1422
[10] Zavt G S, Kalder K A, Kuusmann I L, Lushchik C B, Plekhanov V G, Cholakh S O and Évarestov R A 1976 *Sov. Phys. Solid State* **18** 1588
[11] Plekhanov V G 1996 *Phys. Rev.* **54** 3869
[12] Miki T, Ikeya M, Kondo Y and Kanzaki H 1981 *Solid State Commun.* **39** 647
[13] Ichikawa K, Suzuki N and Tsutsumi K 1981 *J. Phys. Soc. Japan* **50** 3650
[14] Liu D R 1987 *Solid State Commun.* **63** 489
[15] Kunz A B and Mickish D J 1975 *Phys. Rev.* **11** 1700
[16] Baroni S, Pastori Parravicini G and Pezzica G 1985 *Phys. Rev.* **32** 4077
[17] Shirley E 2004 *J. Electron Spectrosc. Relat. Phenom.* **137–40** 579
[18] Schülke W 2001 *J. Phys.: Condens. Matter* **13** 7557
[19] Schülke W 2007 *Electron Dynamics by Inelastic X-Ray Scattering* (*Oxford Series on Synchrotron Radiation* vol 7) (Oxford: Oxford University Press)
[20] Hämäläinen K, Galambosi S, Soininen J A, Shirley E L, Rueff J P and Shukla A 2002 *Phys. Rev.* **65** 155111
[21] Feng Y, Seidler G T, Cross J O, Macrander A T and Rehr J J 2004 *Phys. Rev.* **69** 125402
[22] Galambosi S, Soininen J A, Nygård K, Huotari S and Hämäläinen K 2007 *Phys. Rev.* **76** 195112
[23] Feng Y, Soininen J A, Ankudinov A L, Cross J O, Seidler G T, Macrander A T, Rehr J J and Shirley E L 2008 *Phys. Rev.* **77** 165202
[24] Lima F, Saleta M, Pagliuca R, Eleotério M, Reis R, Júnior J F, Meyer B, Bittar E, Souza-Neto N and Granado E 2016 *J. Synchrotron Rad.* **23** 1538
[25] Rehr J J and Albers R C 2000 *Rev. Mod. Phys.* **72** 621
[26] Soininen J A, Ankudinov A L and Rehr J J 2005 *Phys. Rev.* B **72** 045136
[27] Rehr J J, Kas J J, Vila F D, Prange M P and Jorissen K 2010 *Phys. Chem. Chem. Phys.* **12** 5503
[28] Lazicki A, Loubeyre P, Occelli F, Hemley R J and Mezouar M 2012 *Phys. Rev.* B **85** 054103
[29] Vinson J, Rehr J J, Kas J J and Shirley E L 2011 *Phys. Rev.* B **83** 115106
[30] Gilmore K, Vinson J, Shirley E, Prendergast D, Pemmaraju C, Kas J, Vila F and Rehr J 2015 *Comput. Phys. Commun.* **197** 109
[31] Giannozzi P *et al* 2009 *J. Phys.: Condens. Matter* **21** 395502
[32] Pretzel F, Rupert G, Mader C, Storms E, Gritton G and Rushing C 1960 *J. Phys. Chem. Solids* **16** 10
[33] Sternemann H, Sternemann C, Seidler G T, Fister T T, Sakko A and Tolan M 2008 *J. Synchrotron Rad.* **15** 162
[34] Ribberfors R 1975 *Phys. Rev.* B **12** 2067
[35] Huotari S, Boldrini B, Honkimäki V, Suortti P and Weyrich W 2009 *J. Synchrotron Rad.* **16** 672
[36] Biggs F, Mendelsohn L and Mann J 1975 *At. Data Nucl. Data Tables* **16** 201
[37] Huotari S, Hämäläinen K, Manninen S, Issolah A and Marangolo M 2001 *J. Phys. Chem. Solids* **62** 2205
[38] Holm P and Ribberfors R 1989 *Phys. Rev.* A **40** 6251
[39] Lebègue S, Alouani M, Arnaud B and Pickett W E 2003 *Europhys. Lett.* **63** 562
[40] Priyanga G S, Meenaatci A A, Palanichamy R R and Iyakutti K 2014 *Comput. Mater. Sci.* **84** 206
[41] Chen Y M, Chen X R, Wu Q, Geng H Y, Yan X Z, Wang Y X and Wang Z W 2016 *J. Phys. D: Appl. Phys.* **49** 355305
[42] Olovsson W, Tanaka I, Mizoguchi T, Puschnig P and Ambrosch-Draxl C 2009 *Phys. Rev.* B **79** 041102